Acta Mech 230, 2279–2293 (2019)
https://doi.org/10.1007/s00707-019-02396-w

ORIGINAL PAPER

Lingyun Yao · Guoliang Huang · Hui Chen · Miles V. Barnhart

A modified smoothed finite element method (M-SFEM) for analyzing the band gap in phononic crystals

Received: 12 November 2018 / Revised: 15 February 2019 / Published online: 21 March 2019

Abstract The present work proposes a novel modified smoothed finite element method (M-SFEM) to calculate the band structures of two-dimensional in-plane elastic waves in phononic crystals (PCs). Using the gradient smoothing technique over the cell-based smoothing domains, the cell-based gradient smoothing operation can offer 'proper softening effects' in SFEM modeling. According to the generalized integration rules, by simply shifting integration points to an unconventional location in the mass matrix, the accuracy of the M-SFEM model can be further improved. Numerical examples are presented for PCs using the proposed method for the computation of band gap (BG) frequency regions. The accuracy and efficiency of the modified SFEM are compared with those of the corresponding FEM and SFEM. The advantages of the modified SFEM for computing the BGs in PCs are discussed as compared to the conventional FEM. The results show the performance improvement of the M-SFEM compared to the FEM and SFEM.

1 Introduction

In recent years, phononic crystals (PCs) composed of two or more materials with contrasting mechanical properties have received considerable attention because of their unique and useful dynamic properties [1]. The most interesting property of PCs is the existence of band gaps (BGs) where the propagation of elastic/acoustic waves is prohibited over certain frequency regions. This means that PCs can designate the pass band or band gap frequency ranges in their elastic/acoustic wave transmission spectrum, which leads to an array of potential engineering applications such as vibration isolation and mechanical filters [2,3].

There are two theories to explain the formation mechanism of band gaps in PCs. The traditional theory is based on Bragg scattering where previous research has used mechanical lattice structures to determine the band gaps in PCs [4]. In this situation, the propagating wavelength must be comparable to the crystal lattice constant to create the BGs induced by the Bragg scattering effect. Owing to the demand of the lattice constant, the low-frequency waves would be needed to control for the superstructures [5–8]. This limitation makes the utilization of PCs unrealistic for most practical engineering applications where low-frequency wave attenuation is needed.

The second BG formation mechanism first demonstrated experimentally by Liu et al. [9] is based on the local resonance mechanism which allows for a negative effective mass near the local resonance frequency. Based on this BG formation mechanism, an array of PCs has been presented with unique dynamic properties not found in naturally occurring materials [10–14]. The locally resonant microstructures have to be carefully

L. Yao (✉)
College of Engineering and Technology, Southwest University, Chongqing 400715, People's Republic of China
E-mail: 19831022y@163.com

L. Yao · G. Huang · H. Chen · M. V. Barnhart
Department of Mechanical and Aerospace Engineering, University of Missouri, Columbia, MO 65211, USA

designed based on the specific application; hence, the accurate modeling of the phononic band gaps is an important tool for a broad range of research fields.

To obtain the band structure in PCs [15], different methods, including theoretical and numerical methods, have been developed to calculate the phononic band gaps. The plane wave expansion method (PWE) [16,17] and finite difference time domain method (FDTD) [18,19] have been used to analyze the physical behavior of phononic band gaps. However, the PWE may have difficulties in simulating PCs with highly contrasting elastic properties [20]. Similarly, the weak point of the FDTD method is the treatment of boundaries with complicated structures. There are also numerous other methods such as the multiple scattering theory (MST) method [21], the finite element method (FEM) [22–24], the Dirichlet-to-Neumann map method [25], the boundary element method (BEM) [26,27], and the local radial basis function (RBF) collocation [28–30]. Each of these methods possesses strengths and weaknesses. The MST and the Dirichlet-to-Neumann map methods are only appropriate for circular or spherical scatterers. The BEM involves a singular problem which limits its applications, especially in three-dimensional (3D) cases. Nowadays, FEM is becoming popular for analysis of increasingly complex PCs with arbitrarily shaped scatterers. However, the boundary conditions on the interfaces need many elements, and the dispersion error is a critical issue in current FEM analysis, especially in high-frequency domains, which leads to poor accuracy for the analysis in PCs.

In our opinion, the accuracy of FEM depends on the matching state of the discretized system [31], such as the "stiffness system", "damped system" and "mass system". To obtain the proper stiffness and mass in a discrete model, some researchers have investigated a range of techniques to produce a properly 'softened' stiffness or match the state of the discretized system in the FEM model. Some techniques to reduce dispersion error by modifying the mass and stiffness matrices have been previously proposed [32,33]. Guddati et al. [34] studied the generalized integration rules (GIR) in bilinear rectangular elements by shifting the integration points' locations for acoustic problems, viz. a simple shift of the integration points to unconventional locations of $(\pm\sqrt{2/3},\ \pm\sqrt{2/3})$. This results in a second-order higher accuracy with respect to the dispersion error as compared to the conventional integration scheme. Furthermore, Li et al. [35] presented an alpha finite element method (α-FEM) which was formulated to study the propagation of elastic waves in periodic crystals and demonstrated that α-FEM can consider more realistic stiffness and mass parameters in the analysis of PCs as compared to the FEM. He et al. [36] studied an edge-based gradient smoothed technique to soften the "over-stiff" FEM model and present a modified edge-based smoothed finite element method (modified ES-FEM) to compute the BG in acoustic metamaterials. It was shown that the modified ES-FEM is very effective to minimize the dispersion errors of the BGs for acoustic metamaterials.

As the gradient smoothing technique has been shown to be effective to improve the property of stiffness matrices [36–38], the smoothed finite element method (SFEM) [39–41] was proposed to solve mechanical and acoustic problems with the gradient smoothing technique applied over the cell-based smoothing domains. The cell-based gradient smoothing operation can supply 'proper softening effects' to the FEM model, and so allow the SFEM model to provide much more accurate results in analysis of vibration and acoustic problem [42]. However, SFEM has not yet been applied to the computation of band structures for elastic waves propagating in two-dimensional (2D) PCs.

Motivated by the advantages of GIR and cell-based gradient smoothing operations, in this work, we propose a modified SFEM in cooperation with the unconventional location of $(\pm\sqrt{2/3},\ \pm\sqrt{2/3})$ for mass integration. By shifting integration points to an unconventional location of $(\pm\sqrt{2/3},\ \pm\sqrt{2/3})$ in the mass matrix, the accuracy of the modified SFEM model should be further improved as compared to the model of SFEM and FEM, respectively. Numerical examples will be presented for the computation of dispersion bands in PCs by using the present method. To perform the accuracy and efficiency, the results obtained by FEM and SFEM are also present with compared to the modified SFEM. The strong points of modified SFEM for computing the BGs in PCs are also discussed as compared to the conventional FEM.

The paper is structured as follows. Section 2 briefly introduces the elastic waves in the PCs. Section 3 presents the idea and formulation of the modified SFEM for calculation of dispersion band in PCs. Numerical comparisons are made for the calculation of dispersions bands in PCs in Sect. 4. Finally, a summary and concluding remarks are made in the last section.

2 Band gaps in 2D phononic crystals

A schematic picture of a 2D PC is shown in Fig. 1. It is composed of a square array of straight and infinite quadrangular with a lattice constant denoted as a. Assuming an elastic wave propagating in the isotropic media, the governing equation can be written as

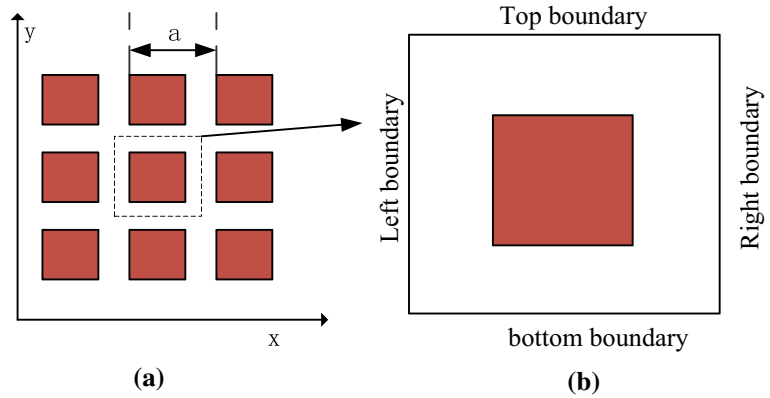

Fig. 1 The considered PCs model **a** the square lattice **b** corresponding square unit cell

$$\frac{\partial \sigma_{i1}}{\partial x_1} + \frac{\partial \sigma_{i2}}{\partial x_2} + \frac{\partial \sigma_{i3}}{\partial x_3} + F_i = \rho \frac{\partial^2 u_i}{\partial t^2}, \tag{1}$$

where σ is the stress, u is the displacement, ρ means the density, and F is the body force. According to Hooke's law, the relationship between the stress $\boldsymbol{\sigma}$ and the strain $\boldsymbol{\varepsilon}$ is expressed as

$$\boldsymbol{\sigma} = \mathbf{D}\boldsymbol{\varepsilon}, \tag{2}$$

where $\mathbf{D}$ is the matrix of material constants. Assume the problem is plane strain problem and interface continuity between the different materials, for the 2D problem (xy-plane); it can be expressed with shear λ and bulk modulus μ as

$$\mathbf{D} = \begin{bmatrix} \lambda + 2\mu & \lambda & 0 \\ \lambda & \lambda + 2\mu & 0 \\ 0 & 0 & \mu \end{bmatrix}, \tag{3}$$

where the first and second Lamé constants are given by $\lambda = \frac{\upsilon E}{(1+\upsilon)(1-2\upsilon)}$; $\mu = \frac{E}{2(1+\upsilon)}$ respectively. The stress and strain vectors can be defined as $\boldsymbol{\sigma} = \{\sigma_x,\ \sigma_y,\ \tau_{xy}\}$; $\boldsymbol{\varepsilon} = \{\varepsilon_x,\ \varepsilon_y,\ \gamma_{xy}\}$. According to the relationship in linear deformation, the strain can be expressed as

$$\varepsilon_x = \frac{\partial u_x}{\partial x}, \quad \varepsilon_y = \frac{\partial u_y}{\partial y}, \quad \gamma_{xy} = \frac{1}{2}\left(\frac{\partial u_x}{\partial y} + \frac{\partial u_y}{\partial x}\right). \tag{4}$$

Substituting Eq. (4) into Eq. (2) yields

$$\sigma_x = (\lambda + 2\mu)\varepsilon_x + \lambda\varepsilon_y, \quad \sigma_y = (\lambda + 2\mu)\varepsilon_y + \lambda\varepsilon_x, \quad \tau_{xy} = \mu\gamma_{xy}. \tag{5}$$

Assuming the body force F zero, substituting Eqs. (2–5) into Eq. (1) yields

$$(\lambda + \mu)\nabla(\nabla.\mathbf{u}) + \mu\nabla^2\mathbf{u} = \rho\ddot{\mathbf{u}}, \tag{6}$$

where $\mathbf{u} = \mathbf{u}_0 \sin(\omega t)$, ω is the angular frequency, then Eq. (6) can be defined in the frequency domain as

$$(\lambda+\mu)\nabla(\nabla.\mathbf{u}_0) + \mu\nabla^2\mathbf{u}_0 + \rho\omega^2\mathbf{u}_0 = 0. \tag{7}$$

Using standard Galerkin procedure with quadrilateral element, the discretized system equations over the entire domain can be expressed in matrix form as

$$(\mathbf{K} - \omega^2\mathbf{M})\mathbf{u} = \mathbf{0}, \tag{8}$$

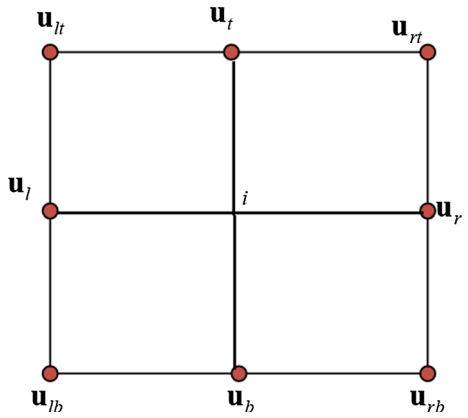

Fig. 2 The unit cell for a 2D periodic structure and illustration of boundary condition

where the matrices $\mathbf{M}$ denotes the assembled global mass matrix of the unit cell, while $\mathbf{K}$ is the stiffness matrix:

$$\mathbf{K} = \int_{\Omega^e} \mathbf{B}^{\mathrm{T}}\mathbf{D}\mathbf{B}\mathrm{d}\Omega, \qquad \mathbf{M} = \int_{\Omega^e} \rho\mathbf{N}^{\mathrm{T}}\mathbf{N}\mathrm{d}\Omega. \tag{9}$$

Here, the cell-based smoothed strain is used to solve the stiffness matrix in the stiffness formulation, which is discussed with more detail in Sect. 3.

Owning to the Bloch theorem, the elastic wave field can be expressed as a periodic function in the PCs structure, reducing the analysis to a single unit cell. The displacement field $\mathbf{u}$ can be described by its relations [43,44] as

$$\begin{aligned} &\mathbf{u}_{\mathrm{r}} = e^{jk_x a}\mathbf{u}_l, \quad \mathbf{u}_t = e^{jk_y a}\mathbf{u}_b, \\ &\mathbf{u}_{\mathrm{rb}} = e^{jk_x a}\mathbf{u}_{lb}, \quad \mathbf{u}_{rt} = e^{j(k_x+k_y)a}\mathbf{u}_{lb}, \quad \mathbf{u}_{lt} = e^{jk_y a}\mathbf{u}_{lb}, \end{aligned} \tag{10}$$

where j is the imaginary number, the subscripts l, r, b, t, and i denote the displacements corresponding to the left, right, bottom, top, and internal nodes of the unit cell, as shown in Fig. 2, respectively. The double subscripts mean the displacements of the corner nodes: for example, lb denotes the left bottom corner. For a hexagonal lattice, the PCs is shown in Fig. 3. The periodic boundary conditions of displacements for the hexagonal unit cell are expressed as [44]

$$\mathbf{u}(\mathrm{x}_{\Gamma_1}) = \mathbf{u}(\mathrm{x}_{\Gamma_4})\mathrm{e}^{-j\left(k_x\frac{\sqrt{3}a}{2}+k_y\frac{a}{2}\right)}, \quad \mathbf{u}(\mathrm{x}_{\Gamma_2}) = \mathbf{u}(\mathrm{x}_{\Gamma_5})\mathrm{e}^{-j(k_y a)}, \quad \mathbf{u}(\mathrm{x}_{\Gamma_3}) = \mathbf{u}(\mathrm{x}_{\Gamma_6})e^{j\left(k_x\frac{\sqrt{3}a}{2}-k_y\frac{a}{2}\right)}. \tag{11}$$

According to the Bloch theorem, it can be defined the following transformation as

$$\mathbf{u} = \mathbf{T}\tilde{\mathbf{u}}, \qquad \mathbf{T} = \begin{bmatrix} \mathbf{I} & \mathbf{0} & \mathbf{0} & \mathbf{0} \\ \mathbf{I}e^{k_x a} & \mathbf{0} & \mathbf{0} & \mathbf{0} \\ \mathbf{0} & \mathbf{I} & \mathbf{0} & \mathbf{0} \\ \mathbf{0} & \mathbf{I}e^{k_y a} & \mathbf{0} & \mathbf{0} \\ \mathbf{0} & \mathbf{0} & \mathbf{I} & \mathbf{0} \\ \mathbf{0} & \mathbf{0} & \mathbf{I}e^{k_x a} & \mathbf{0} \\ \mathbf{0} & \mathbf{0} & \mathbf{I}e^{k_y a} & \mathbf{0} \\ \mathbf{0} & \mathbf{0} & \mathbf{I}e^{(k_x+k_y)a} & \mathbf{0} \\ \mathbf{0} & \mathbf{0} & \mathbf{0} & \mathbf{I} \end{bmatrix}, \qquad \tilde{\mathbf{u}} = \begin{bmatrix} \mathbf{u}_l \\ \mathbf{u}_b \\ \mathbf{u}_{lb} \\ \mathbf{u}_i \end{bmatrix}. \tag{12}$$

Substituting the transformation (12) into the governing equations in Eq. (8) results in the reduced coordinates

$$(\mathbf{T}^{\mathrm{H}}(\mathbf{K} - \omega^2\mathbf{M})\mathbf{T})\tilde{\mathbf{u}} = \mathbf{0}, \tag{13}$$

where the superscript H denotes the Hermitian transpose. Using symbol $\mathbf{D}$ to represent the expression of $\mathbf{T}^{\mathrm{H}}(\mathbf{K} - \omega^2\mathbf{M})\mathbf{T}$, Eq. (13) can be written to give the following eigenvalue problem:

$$\mathbf{D}(k_x, k_y, \omega)\tilde{\mathbf{u}} = \mathbf{0}. \tag{14}$$

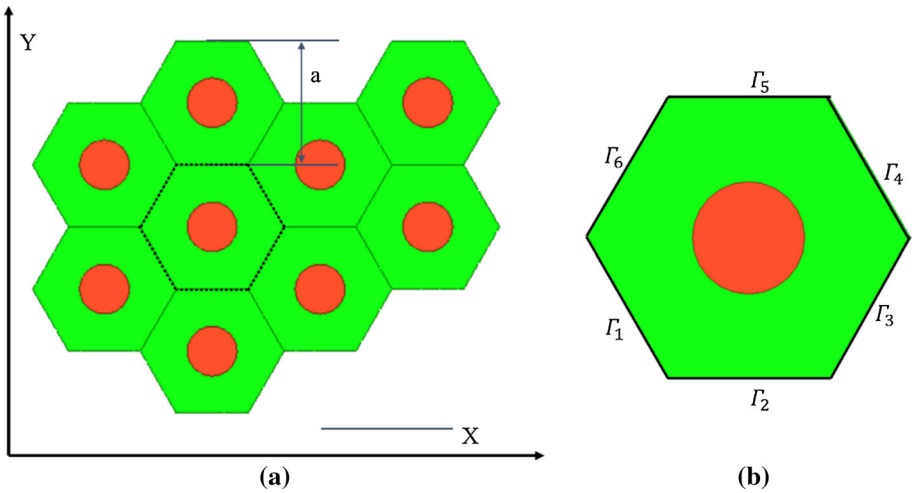

Fig. 3 The considered PCs model **a** the hexagonal lattice **b** corresponding hexagonal unit cell

Because each pair of (k_x, k_y) can describe the frequencies of propagating waves, the results of the dispersion bands can subsequently be obtained. As the study introduced, the BGs will exist in the PCs when two dispersion surfaces do not overlap [44].

3 SFEM for smoothed stiffness in the model of phononic crystals

This section gives a brief introduction of the cell-based smoothing technique for calculating the smoothed stiffness matrix $\overline{\mathbf{K}}$ instead of the stiffness matrix $\mathbf{K}$ given in Eq. (13). In SFEM model, the cell-based smoothing operation is performed to the gradient of displacement for each smoothing cell in an element. Firstly, the unit cell is discretized into N_e quadrilateral elements containing N_d nodes, each element domain Ω is cut into a number *of* smoothing cells [39], *SC* denotes the number of smoothing cells, meeting the demand of $\Omega_1 \cup \Omega_2 \cup ...\Omega_{SC} = \Omega$ and $\Omega_1 \cap \Omega_2 \cap ...\Omega_{SC} = \emptyset$, shown in Fig. 4. Experience indicates that the optimal number of *SC* is 3 or 4 for acoustic problems [40].

Applying the smoothing operation on the strain, the compatible strain in *C-th* smoothing domain can be solved as [39]

$$\bar{\boldsymbol{\varepsilon}}_C(\mathbf{x}) = \frac{1}{A_C}\int_{\Omega_C} \nabla s\mathbf{u}^h(\mathbf{x})\mathrm{d}\Omega_C = \frac{1}{A_C}\int_{\Gamma_C} \mathbf{n}_C\mathbf{u}^h(\mathbf{x})\mathrm{d}\Gamma_C = \sum_{I=1}^{Np} \bar{\mathbf{B}}_I^C(\mathbf{x})\mathbf{d}_I, \tag{15}$$

where Γ_c is the smoothed cell boundary, $\mathbf{n}_C$ notes the outward normal vector matrix on the boundary Γ_c, and ∇s means a differential operator matrix defined as

$$\nabla s = \begin{bmatrix} \frac{\partial}{\partial x} & 0 \\ 0 & \frac{\partial}{\partial y} \\ \frac{\partial}{\partial y} & \frac{\partial}{\partial x} \end{bmatrix}. \tag{16}$$

In Eq. (14), $\mathbf{u}^h(\mathbf{x})$ is the displacement vector written as

$$\mathbf{u}^h(\mathbf{x}) = \sum_{I=1}^{Np} \mathbf{N}_I(\mathbf{x})\mathbf{d}_I, \tag{17}$$

where N_p is the nodes number in the element, $\mathbf{d}_I = [u_I, v_I]^T$ is the generalized nodal displacement at node I, and $\mathbf{N}_I(\mathbf{x})$ is the shape functions

$$\mathbf{N}_I(\mathbf{x}) = \mathrm{diag}(N_I(\mathbf{x}), N_I(\mathbf{x})). \tag{18}$$

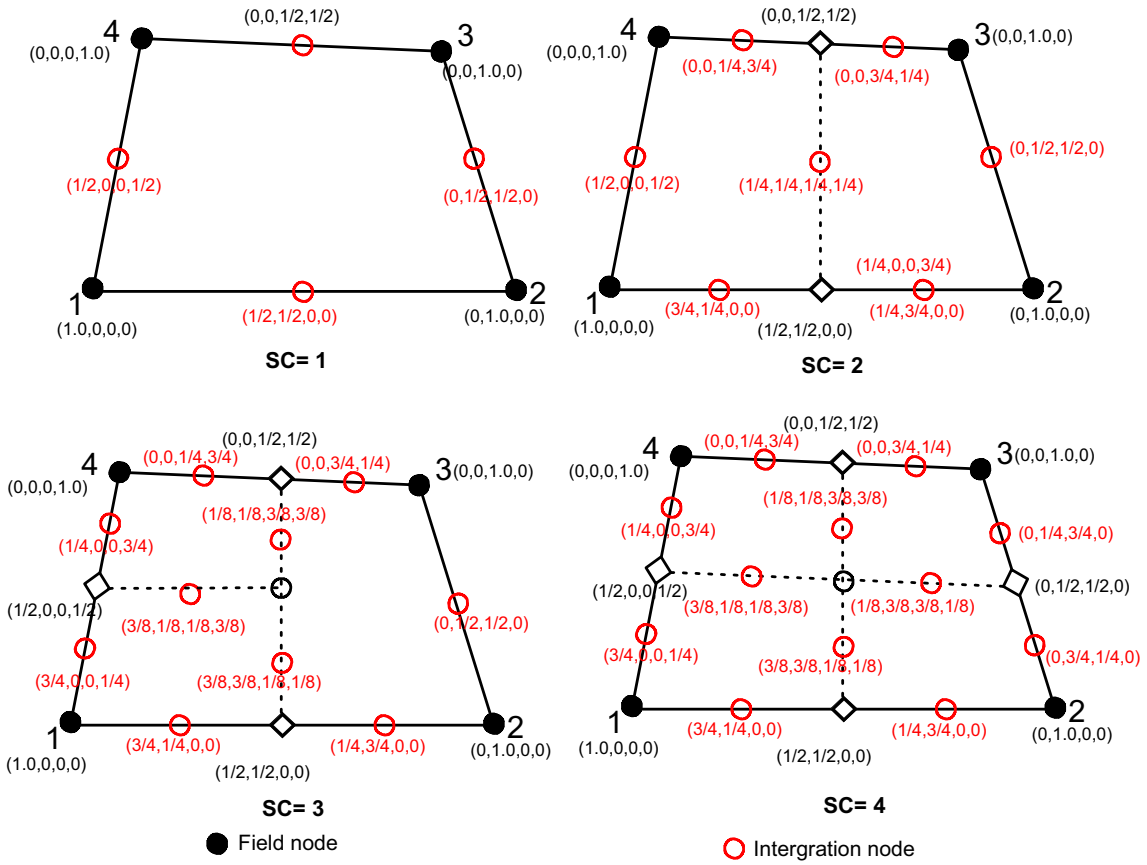

Fig. 4 Division of element into smoothing cells (SC) and the value of shape functions along cell boundaries

In Eq. (18), $N_I(\mathbf{x})$ is the shape function associated with node$I$.

The smoothed strain matrix, $\bar{\mathbf{B}}_I^C(\mathbf{x})$, can be defined as

$$\overline{\mathbf{B}}_I^c(\mathbf{x}) = \frac{1}{A_C}\int_{\Gamma_C}\begin{pmatrix} N_I n_x & 0 \\ 0 & N_I n_y \\ N_I n_y & N_I n_x \end{pmatrix} \mathrm{d}\Gamma. \tag{19}$$

According to the smoothing strain, $\bar{\boldsymbol{\varepsilon}}_C$, in Eq. (2), the smoothed stiffness matrix $\bar{\mathbf{K}}$ can be obtained as

$$\overline{\mathbf{K}} = \sum_{C=1}^{\mathrm{SC}} (\overline{\mathbf{B}}_I^C)^T \mathbf{D}\overline{\mathbf{B}}_I^C A_C. \tag{20}$$

4 Formulation of modified mass matrix in the phononic crystals model

Since finite elements can be distorted, it is customary to map the finite elements from a square parent element $(-1 < \xi < 1, \quad -1 < \eta < 1)$, ζ and η denotes the coordinates in the natural (parent) element. The present work transforms the integrals into the natural coordinate system as

$$\mathbf{M}_e = \int_{-1}^{+1}\int_{-1}^{+1} \mathbf{N}^{\mathbf{T}}\mathbf{N}\det(\mathbf{J})\mathrm{d}\xi\,\mathrm{d}\eta. \tag{21}$$

Like [34], using generalized integration rules to parameterize Gauss point's location, Eq. (21) can be redefined as

$$\mathbf{m}_e = \sum_{i=1}^{4} W_i^{\mathbf{M}} (\mathbf{N}(\xi_i^{\mathbf{M}}, \eta_i^{\mathbf{M}}))^{\mathrm{T}} \mathbf{N}(\xi_i^{\mathbf{M}}, \eta_i^{\mathbf{M}}) \det(\mathbf{J}), \tag{22}$$

where $W_i^{\mathbf{M}}$ are the weights and $(\xi_i^{\mathbf{M}}, \eta_i^{\mathbf{M}})$ are the local coordinates of the Gauss points.

A conventional 2×2 Gauss rule ($W_i^{\mathbf{M}} = 1$; $\xi_i^{\mathbf{M}} = \pm\sqrt{1/3}$, $\eta_i^{\mathbf{M}} = \pm\sqrt{1/3}$) is used to solve the matrix. However, the previous research [34] indicates that the matching state of the discretized system can be well realized by simply shifting integration points to unconventional locations of $(\pm\sqrt{2/3}, \pm\sqrt{2/3})$ in the process of matrix calculation.

In the present work, we use the unconventional locations of $(\pm\sqrt{2/3}, \pm\sqrt{2/3})$ to calculate the mass matrix of the PCs element, and then a modified mass matrix is proposed to balance the smoothed stiffness which is created by SFEM. In numerical examples, the accuracy and convergence rate of the proposed algorithm is studied in detail.

5 Numerical applications

In this section, numerical examples are studied in detail to investigate the prediction accuracy of the band gap formation in PCs. For comparing the computational cost (time and memory requirements), the present computations using MATLAB code were performed on a PC system with 8 GB of RAM and 2.30 GHz CPU speed.

5.1 A square lattice with square scatterers

In this subsection, lead (Pb) columns embedded in an epoxy matrix are considered as shown in Fig. 5. The lattice constant is $a = 0.10$ m, and the dimension of the Pb columns with square cross-section is $b = 0.06$ m. Figure 5 shows the first irreducible Brillouin zone and the corresponding square unit cell. The corresponding material properties for the Pb columns are given as: density $\rho_{\mathrm{Pb}} = 11{,}600$ kg/m^3, Lamé constants $\lambda_{\mathrm{Pb}} = 4.23 \times 10^{10}$, $\mu_{\mathrm{Pb}} = 1.49 \times 10^{10}$. The material properties of the epoxy matrix are defined as: $\rho_{\mathrm{epo}} = 1180$ kg/m^3, Lamé constants $\lambda_{\mathrm{epo}} = 4.43 \times 10^9$, $\mu_{\mathrm{epo}} = 1.59 \times 10^9$.

Figure 6 shows the mesh distribution of the unit cell for the Pb/epoxy phononic crystal. The 10×10 meshes are uniformly distributed over the unit cell. To quantitatively study the numerical solutions, the general estimate for natural frequencies' errors is defined as

$$e(\mathrm{freq}) = \frac{\left| f^{\mathrm{exact}} - f^h \right|}{f^{\mathrm{exact}}}, \tag{23}$$

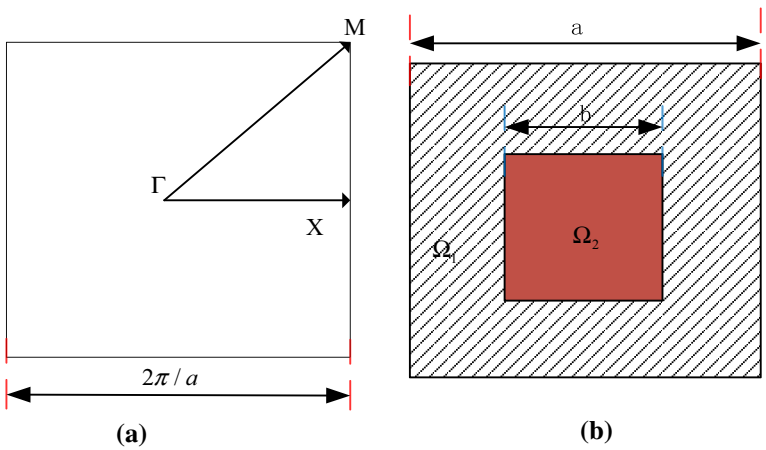

Fig. 5 **a** The first irreducible Brillouin zone and **b** corresponding square unit cell with square scatterers

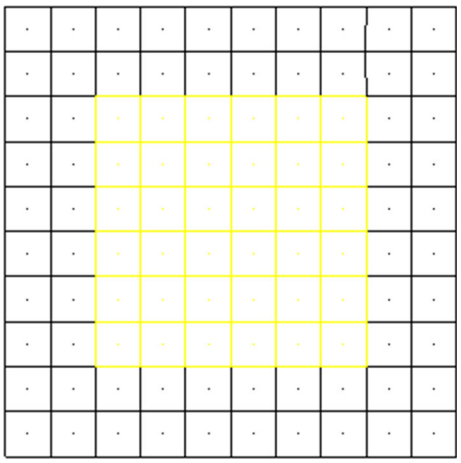

Fig. 6 Mesh distribution of the PC in a square lattice with square scatterers

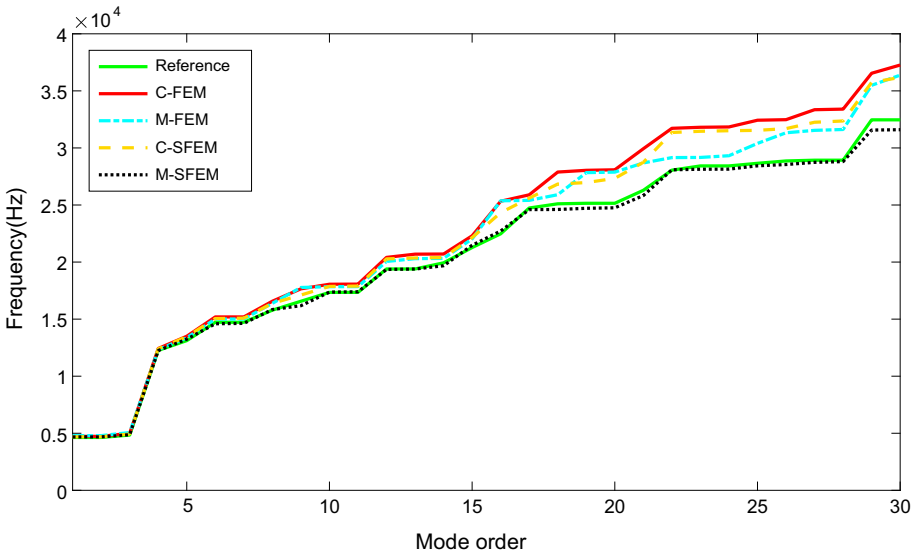

Fig. 7 Natural frequencies of the first 30 modes at wave vector of M for C-FEM, M-FEM, SFEM, and M-SFEM

where f is the modal frequency. The superscript *exact* represents the exact or reference solution. The superscript h denotes the solution obtained using a numerical method including the present M-SFEM, C-FEM (using conventional Gauss integration points) and M-FEM (using unconventional Gauss integration points) with the same meshes.

Using the model shown in Fig. 6, the natural frequencies of the first 30 modes along the **M** direction, **X** direction by C-FEM, M-FEM and M-SFEM are shown in Figs. 7 and 8, respectively. To make a comparison, a reference solution using a very fine mesh (10,121 nodes and 10,000 elements) is obtained using the software package COMSOL Multiphysics [45]; the version is COMSOL Multiphysics 5.2. It is found that the solutions from the M-SFEM corresponding to the integration point with an unconventional location of $(\pm\sqrt{2/3}, \pm\sqrt{2/3})$ are much better than the solutions obtained from FEM using conventional or unconventional integration locations. Furthermore, the M-SFEM results are even better than the results obtained from SFEM using the conventional location of $(\pm\sqrt{1/3}, \pm\sqrt{1/3})$, as shown in Figs. 7 and 8. The mass matrix obtained from the conventional integration location for both FEM and SFEM shows weaker results as compared to unconventional location strategies of the mass matrix.

The numerical solutions of the **X–Y** mode using conventional FEM (C-FEM), unconventional FEM (MR-FEM) are both presented in Fig. 9. Those from the conventional (C-SFEM) and modified FEM (M-SFEM) are both presented in Fig. 10. It can be found from these figures that the accuracy of the unconventional

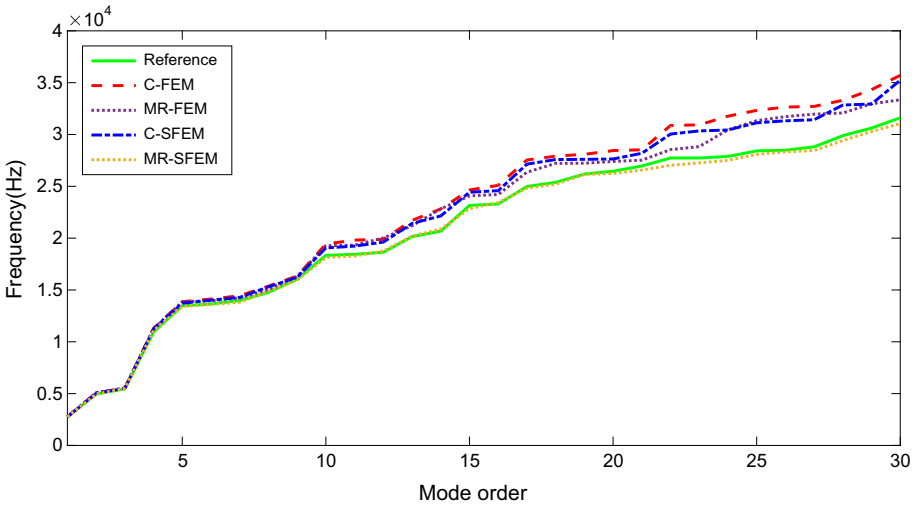

Fig. 8 Natural frequencies of the first 30 modes at the wave vector of X for C-FEM, M-FEM, SFEM, and M-SFEM

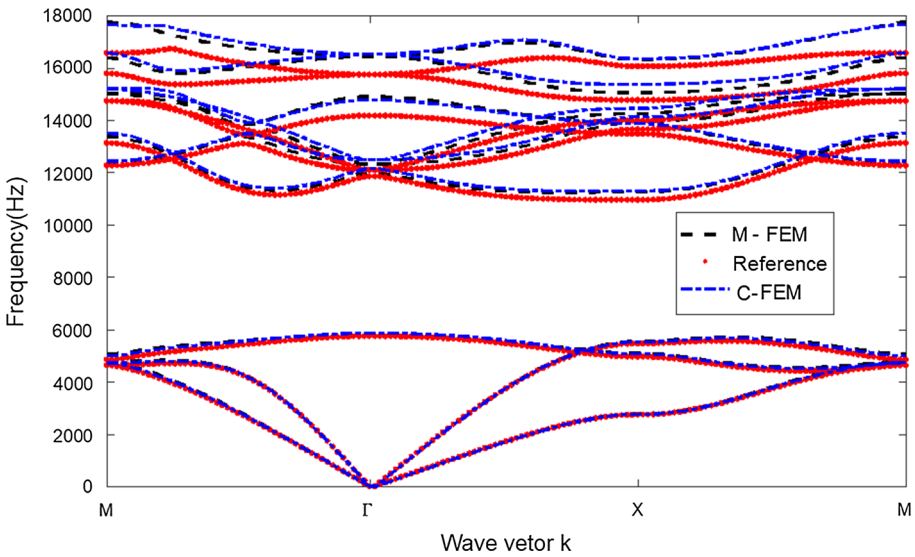

Fig. 9 Numerical solutions of X–Y modes using conventional and modified FEM

FEM, conventional FEM, conventional SFEM and modified SFEM (M-SFEM), are both dependent on the frequency value. As the frequency becomes higher, the accuracy of the models is reduced. Another observation is that the accuracy of the modified SFEM (M-SFEM) is much better than for the corresponding conventional FEM, conventional SFEM (C-SFEM) and modified FEM (MR-FEM). For a more detailed investigation, the convergence rates of the different numerical methods for various modes are given in Fig. 11. We can see from the figure that the modified SFEM consistently demonstrates the best accuracy in comparison to the conventional or modified FEM and conventional SFEM.

In order to investigate the computational cost for this numerical example, the work also presents the CPU time and memory usage. The CPU times of the C-FEM and M-FEM are both the same, 54.4 s, while the CPU times of the SFEM and M-SFEM are both the same, 23.6 s. The memory usage of these methods is the same because the element number is not changed. Because of the cell-based smoothing technique, the computational efficiency of SFEM is higher than that of C-FEM. While the M-SFEM just changes the integration location for the system matrix, there is no change in computational efficiency of SFEM. Hence, the computational cost of SFEM or M-SFEM is lower than that of C-FEM or M-FEM.

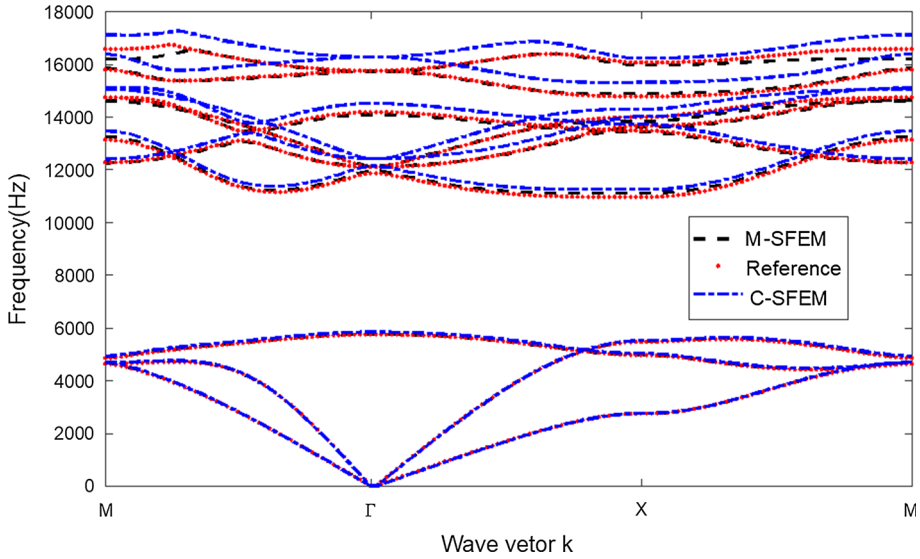

Fig. 10 Numerical solutions of the X–Y modes using conventional and modified SFEM

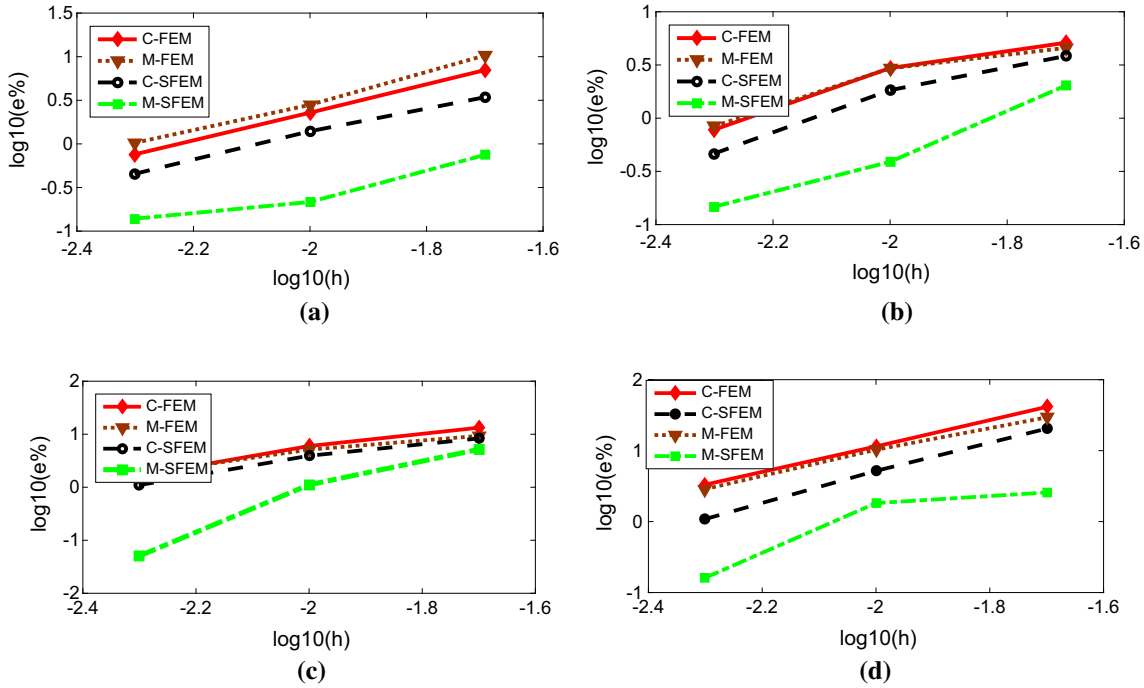

Fig. 11 Comparison of convergence rates for different numerical methods over the wave vector of X **a** Mode 2, **b** Mode 5, **c** Mode 10, **d** Mode 30

5.2 A square lattice with circular-shaped scatterers

Now we consider a binary locally resonant acoustic metamaterial (LRAM) with a lattice constant of $a = 0.2$ m, and unit cells consisting of epoxy with embedded rubber cylinders of radius $r = 50$ mm as shown in Fig. 12. In the simulation, the material properties used for the epoxy are the same as those given previously, while the density of the rubber, and the first and second Lamé constants are defined as $\rho_{\text{rub}} = 1300\,\text{kg/m}^3$, $\lambda_{\text{rub}} = 6 \times 10^5$ and $\mu_{\text{rub}} = 4 \times 10^4$, respectively.

The dispersion curves of the first ten modes are shown in Fig. 13 and were obtained using the modified SFEM with a coarse mesh (478 nodes 437 quadrilateral elements). To provide a comparison, the results obtained

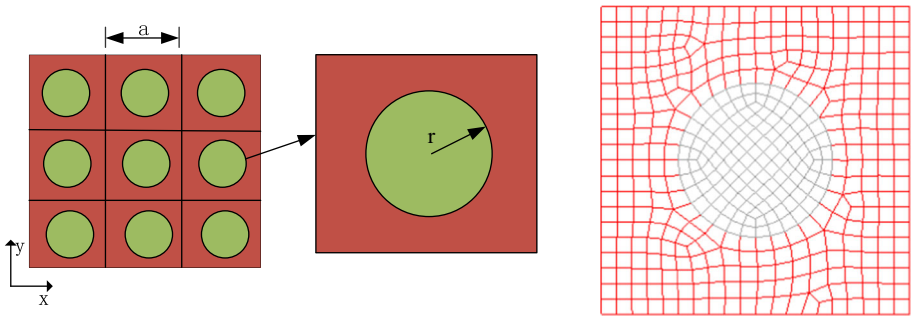

Fig. 12 **a** Corresponding square unit cell with circular-shaped scatterers, **b** mesh model

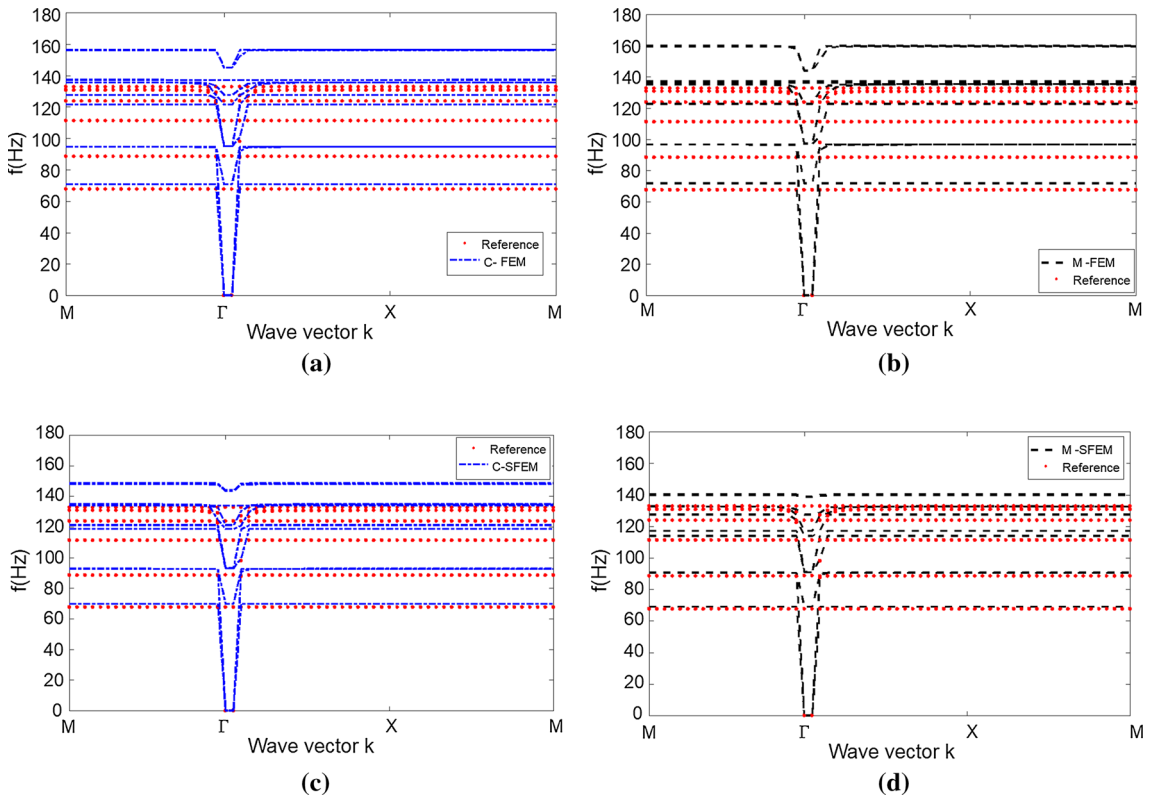

Fig. 13 Comparison of the dispersion band solutions obtained using different numerical methods. **a** Conventional FEM (C-FEM), **b** Modified FEM (MR-FEM), **c** Conventional SFEM (C-SFEM), **d** Modified SFEM (M-SFEM)

from the conventional FEM, modified FEM and conventional SFEM with the same meshes are also shown in this figure. The reference results are once again obtained from COMSOL Multiphysics 5.2 with a very fine mesh (47,681 nodes with 21,684 quadrilateral elements) and are also given in this figure. Excellent agreement is observed in Fig. 13d between the modified SFEM using a coarse mesh (478 nodes 437 quadrilateral elements) and the reference results from COMSOL [45]. This demonstrates that the modified SFEM is a very effective tool for obtaining accurate dispersion bands for the metamaterial unit cell considered. Furthermore, a large deviation between the conventional FEM (C-FEM) using a coarse mesh and the reference result is observed in Fig. 13a, which is even more obvious in the higher modes. Compared to the conventional FEM, the results from the modified FEM in Fig. 13b and conventional SFEM in Fig. 13c show higher accuracy. However, these results are significantly worse than the modified SFEM results.

A comparison of the relative error over the wave vector **M** using different numerical methods is shown in Fig. 14. Again, it is found that the modified SFEM performs significantly better in comparison with the other

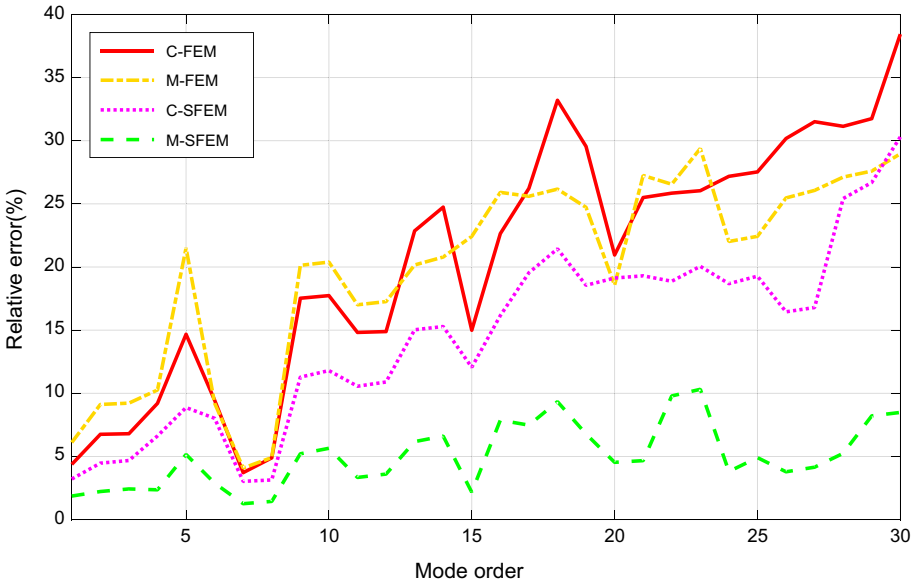

Fig. 14 Comparison of relative error at wave vector along direction **M.**

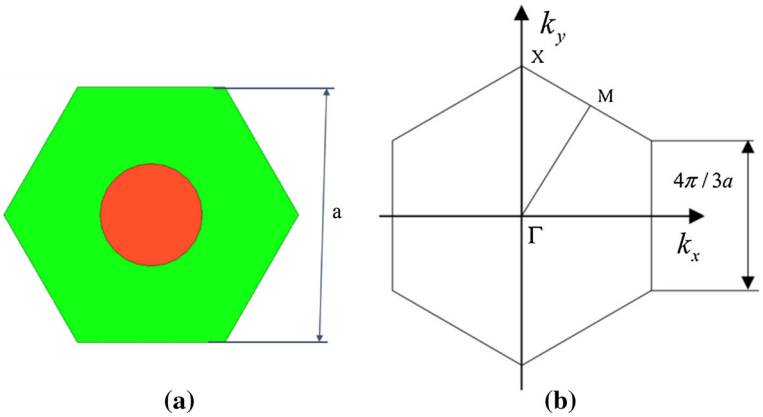

Fig. 15 **a** The first irreducible Brillouin zone, **b** corresponding hexagonal unit cell with circular-shaped scatterers

numerical methods considered, and the conventional FEM shows the highest error for both lower and higher order modes. Furthermore, the errors continue to increase as the mode order increases.

5.3 A hexagonal lattice with circular scatterers

To test the present M-SFEM for other lattice geometries, now the authors consider a hexagonal lattice with circular-shaped scatterers embedded in the epoxy matrix. Figure 14 shows the first irreducible Brillouin zone and the corresponding hexagonal unit cell. The lattice constant is defined as $a = 0.1$ m, and the radius of the cylindrical Pb scatterers is $r = 0.02$ m. Figure 15 shows the numerical results of the band diagrams obtained using the conventional FEM, modified FEM, conventional SFEM and modified SFEM with the same coarse mesh (465 nodes, 428 quadrilateral elements). The reference solutions are again obtained using commercial FEM software COMSOL (14,585 nodes, 12,458 quadrilateral elements). As expected, the numerical solutions obtained from the M-SFEM have the best agreement with the reference solution.

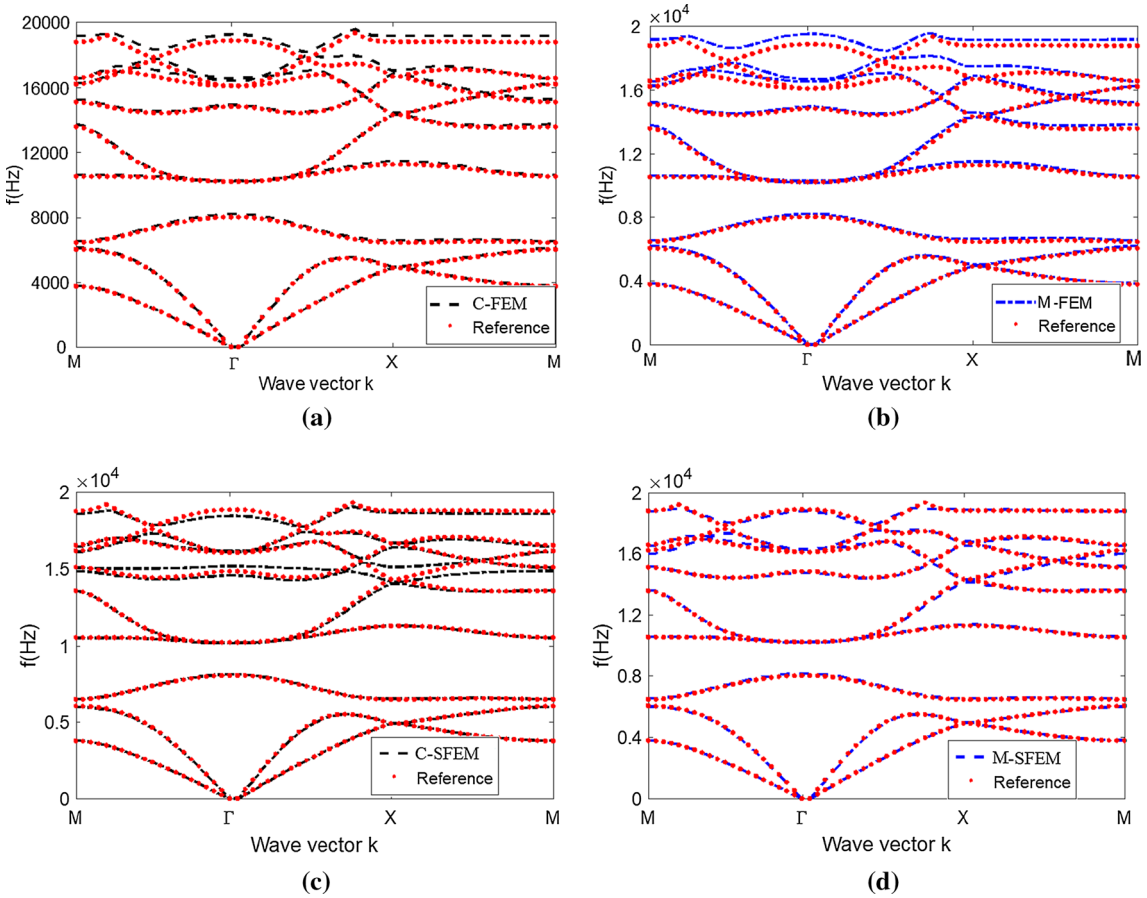

Fig. 16 Comparison of band structures using different numerical methods. **a** Conventional FEM (C-FEM), **b** modified FEM (M-FEM), **c** conventional SFEM(C-SFEM), **d** Modified SFEM (M-SFEM)

6 Conclusions

In this work, a modified smoothed finite element model is introduced to study the elastic wave propagation in phononic crystals by incorporating the unconventional location of $(\pm\sqrt{2/3}, \pm\sqrt{2/3})$ for mass integration and a cell-based smoothed stiffness technique. By simply shifting integration points to unconventional locations of $(\pm\sqrt{2/3}, \pm\sqrt{2/3})$ in the mass matrix, the accuracy of the modified SFEM (M-SFEM) model is higher than for the FEM and SFEM. Numerical examples are presented for PCs to demonstrate the advantages of the M-SFEM. Some conclusions can be derived such as:

1. Like the C-FEM, M-FEM and SFEM, the M-SFEM gives poor solutions to analyze the band gaps in phononic crystals for high frequencies.
2. Compared to M-FEM, C-FEM and conventional SFEM, the M-SFEM, incorporating the unconventional locations of $(\pm\sqrt{2/3}, \pm\sqrt{2/3})$ for mass integration and a cell-based smoothed stiffness technique, can offer a softened model compared with the C-FEM and M-FEM. It can also match the state of the smoothed stiffness and mass matrices and thus gives much better solutions than those obtained using C-FEM and M-FEM and conventional SFEM.
3. Like the C-FEM, M-FEM and SFEM, the M-SFEM can easily be extended to solve fluid/solid or solid/fluid phononic crystals with fluid–structure interaction (FSI). In the future, the M-SFEM can also be extended to solve three-dimensional phononic crystals, even to calculate the electromagnetic band gaps problems.

Acknowledgements This work was supported by the National Natural Science Foundation of China (No. 51605391), the Chongqing Science & Technology Commission (CSTC) (No. 2015JCYJA60008), the Fundamental Research Funds for the Central Universities (No. XDJK2019B020)

References

1. Kushwaha, M.S., Halevi, P., Dobrzynski, L., Djafarirouhani, B.: Acoustic band-structure of periodicelastic composites. Phys. Rev. Lett. **71**, 2022–2025 (1993)
2. Liu, Z.Y., Chan, C.T., Sheng, P.: Analytic model of phononic crystals with local resonances. Phys. Rev. B. **71**(1), 014103 (2005)
3. Poulton, C.G., Movchan, A.B., McPhedran, R.C., Nicorovici, N.A., Antipov, Y.A.: Eigenvalue problems for doubly periodic elastic structures and phononic band gaps. Proc. R.Soc. A Math. Phys. **456**, 2543–2559 (2000)
4. Martinsson, P.G., Movchan, A.B.: Vibrations of lattice structures and phononic band gaps. Q. J. Mech. Appl. Math. **56**, 45–64 (2003)
5. Huang, H.H., Sun, C.T., Huang, G.L.: On the negative effective mass density in acoustic metamaterials. Int. J. Eng. Sci. **47**(4), 610–617 (2009)
6. Liu, Y., Su, X., Sun, C.T.: Broadband elastic metamaterial with single negativity by mimicking lattice systems. J. Mech. Phys. Solids **74**, 158–174 (2015)
7. Chen, Y.Y., Huang, G.L., Sun, C.T.: Band gap control in an active elastic metamaterial with negative capacitance piezoelectric shunting. J. Vib. Acoust. Trans. ASME **136**, 061008 (2014)
8. Wu, J., Luo, Z., Li, H., Zhang, N.: Level-set topology optimization for mechanical metamaterials under hybrid uncertainties. Comput. Methods Appl. Mech. Eng. **319**, 414–441 (2017)
9. Liu, Z., Zhang, X., Mao, Y., Zhu, Y.Y., Yang, Z., Chan, C.T., Sheng, P.: Locally resonant sonic crystal. Science **289**, 1734–1736 (2000)
10. Huang, G.L., Sun, C.T.: Modeling heterostructures of nano-phononic crystals by continuum model with microstructures. Appl. Phys. Lett. **88**, 261908 (2006)
11. Guillén-Gallegos, C., Alva-Medrano, H., Pérez-Aguilar, H., Mendoza-Suárez, A., Villa-Villa, F.: Phononic band structure of an acoustic waveguide that behaves as a phononic crystal. Results Phys. **12**, 1111–1118 (2019)
12. Wang, G., Wen, X., Wen, J.H., Shao, L., Liu, Y.: Two-dimensional locally resonant phononic crystals with binary structures. Phys. Rev. Lett. **93**, 154302 (2004)
13. Krushynska, A.O., Kouznetsova, V.G., Geers, M.G.D.: Towards optimal design of locally resonant acoustic metamaterials. J. Mech. Phys. Solids **71**, 179–196 (2014)
14. Veres, I.A., Berer, T., Matsuda, O.: Complex band structures of two dimensional phononic crystals: analysis by the finite element method. J. Appl. Phys. **114**, 083519 (2013)
15. Huang, Y.Q., Li, J.C., Yang, W.: Modeling backward wave propagation in metamaterials by the finite element time-domain method. SIAM J. Sci Comput. **35**, B248–B274 (2013)
16. Cao, Y.J., Hou, Z.L., Liu, Y.Y.: Convergence problem of plane-wave expansion method for phononic crystals. Phys. Lett. A **327**, 247–253 (2004)
17. Xiao, S.S., Shen, L.F., He, S.L.: A plane-wave expansion method based on the effective medium theory for calculating the band structure of a two-dimensional photonic crystal. Phys. Lett. A **313**, 132–138 (2003)
18. Zhao, Y., Belov, P., Hao, Y.: Accurate modelling of left-handed metamaterials using a finite-difference time-domain method with spatial averaging at the boundaries. J. Opt. A Pure Appl. Opt. **9**, S468–S475 (2007)
19. Wang, G., Wen, J.H., Han, X.Y., Zhao, H.G.: Finite difference time domain method for the study of band gap in two-dimensional phononic crystals. Acta Phys. Sin. Ed. **52**, 1943–1947 (2003)
20. Shi, S.Y., Chen, C.H., Prather, D.W.: Plane-wave expansion method for calculating band structure of photonic crystal slabs with perfectly matched layers. J. Opt. Soc. Am. A **21**, 1769–1775 (2004)
21. Kafesaki, M., Economou, E.N.: Multiple-scattering theory for three-dimensional periodic acoustic composites. Phys. Lett. B **60**, 11993–2001 (1999)
22. Axmann, W., Kuchment, P.: An efficient finite element method for computing spectra of photonic and acoustic band-gap materials: I. Scalar case. J. Comput. Phys. **150**, 468–481 (1999)
23. Li, J., Wood, A.: Finite element analysis for wave propagation in double negative metamaterials. J. Sci. Comput. **32**(2), 263–286 (2007)
24. Li, J.: Error analysis of mixed finite element methods for wave propagation in double negative metamaterials. J. Comput. Appl. Math. **209**, 81–96 (2007)
25. Wu, Y.M., Lu, Y.Y.: Dirichlet-to-Neumann map method for analyzing interpenetrating cylinder arrays in a triangular lattice. J. Opt. Soc. Am. B **25**, 1466–1473 (2008)
26. Gao, H.F., Xiang, J.W., Zheng, C.J., Jiang, Y.Y.: BEM-based analysis of elastic banded material by using a contour integral method. Eng. Anal. Bound Elem. **53**, 56–64 (2015)
27. Li, F., Wang, Y., Zhang, C.: A BEM for band structure and elastic wave transmission analysis of 2D phononic crystals with different interface conditions. Int. J. Mech. Sci. **144**, 110–117 (2018)
28. Zheng, H., Zhang, C.Z., Wang, Y.S., Sladek, J., Sladek, V.: Band structure computation of in-plane elastic waves in 2D phononic crystals by a meshfree local RBF collocation method. Eng. Anal. Bound Elem. **66**, 77–90 (2016)
29. Zheng, H., Zhang, C.Z., Wang, Y.S., Sladek, J., Sladek, V.: A meshfree local RBF collocation method for anti-plane transverse elastic wave propagation analysis in 2D phononic crystals. J. Comput. Phys. **305**, 997–1014 (2016)
30. Zheng, H., Zhang, C.Z., Zhang, C., Tyrer, M.: A local radial basis function collocation method for band structure computation of phononic crystals with scatterers of arbitrary geometry. Appl. Math Model. **60**, 447–459 (2018)
31. He, Z.C., Liu, G.R., Zhong, Z.H., Wu, S.C., Zhang, G.Y., Cheng, A.G.: An edge-based smoothed finite element method (ES-FEM) for analyzing three-dimensional acoustic problems. Comput. Method Appl. Mech. Eng. **199**, 20–33 (2009)
32. Idesman, A.: Optimal reduction of numerical dispersion for wave propagation problems. Part 1: application to 1-D isogeometric elements, Comput. Method Appl. Mech. Eng. **317**, 970–992 (2017)
33. Idesman, A., Pham, D.: Finite element modeling of linear elastodynamics problems with explicit time-integration methods and linear elements with the reduced dispersion error. Comput. Method Appl. Mech. Eng. **271**, 86–108 (2014)

34. Guddati, M.N., Yue, B.: Modified integration rules for reducing dispersion error in finite element methods. Comput. Method Appl. Mech. Eng. **193**(3–5), 275–287 (2004)
35. Li, E., He, Z.C., Wang, G.: An exact solution to compute the band gap in phononic crystals. Comput. Mater. Sci. **122**, 72–85 (2016)
36. He, Z.C., Li, E., Wang, G., Li, G.Y., Xia, Z.: Development of an efficient algorithm to analyze the elastic wave in acoustic metamaterials. Acta Mech. **227**, 3015–3030 (2016)
37. Li, E., He, Z.C., Wang, G., Liu, G.R.: An efficient algorithm to analyze wave propagation in fluid/solid and solid/fluid phononic crystals. Comput. Method Appl. Mech. Eng. **333**, 421–442 (2018)
38. Wang, G., Cui, X.Y., Feng, H., Li, G.Y.: A stable node-based smoothed finite element method for acoustic problems. Comput. Method Appl. Mech. Eng. **297**, 348–370 (2015)
39. Dai, K.Y., Liu, G.R.: Free and forced vibration analysis using the smoothed finite element method (SFEM). J. Sound. Vib. **301**, 803–820 (2007)
40. Liu, G.R., Nguyen, T.T.: Smoothed Finite Element Methods. CRC Press, Boca Raton (2010)
41. Liu, G.R., Dai, K.Y., Nguyen, T.T.: A smoothed finite element method for mechanics problems. Comput. Mech. **39**, 859–877 (2007)
42. Yao, L.Y., Yu, D.J., Cui, X.Y.: Numerical treatment of acoustic problems with the smoothed finite element method. Appl. Acoust. **71**, 743–753 (2010)
43. Phani, A.S., Woodhouse, J., Fleck, N.A.: Wave propagation in two-dimensional periodic lattices. J. Acoust. Soc. Am. **119**(4), 1995–2005 (2006)
44. Fu, Z.J., Chen, W., Wen, P., Zhang, C.Z.: Singular boundary method for wave propagation analysis in periodic structures. J. Sound. Vib. **425**(7), 170–188 (2018)
45. COMSOL 3.4a, The COMSOL Group, Stockholm, Sweden